JOC Article
pubs.acs.org/joc

# Exploring Photoinduced Decarboxylation Mechanism of *o*-Acetylphenylacetic Acid from the Combined CASSCF and DFT Studies

Lina Ding and Wei-Hai Fang*

*Department of Chemistry, Beijing Normal University, Beijing 100875, People's Republic of China*

*fangwh@bnu.edu.cn*

*Received December 7, 2009*

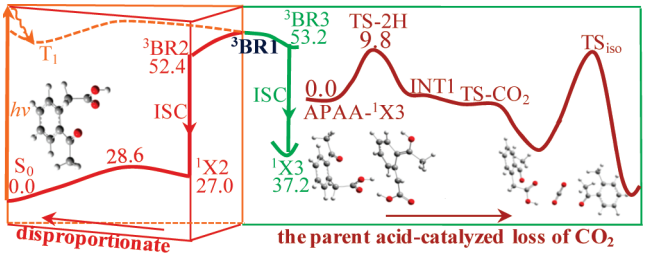


In the present work, we studied the near-UV photoinduced decarboxylation of *o*-acetylphenylacetic acid with complete active space self-consistent field and density functional theory. It was found that irradiation at ~300 nm results in *o*-acetylphenylacetic acid in the $S_1(^1n\pi^*)$ state, which is followed by a rapid relaxation and efficient intersystem crossing to the $T_1(^3n\pi^*)$ state via the $S_1/T_2/T_1$ three-surface intersection. The 1,5-H shift has a barrier of 1.9 kcal·mol$^{-1}$ on the $T_1$ pathway to the triplet 1,4-biradical, which is in good agreement with a rate constant of about $10^{10}$ s$^{-1}$ inferred experimentally for *o*-alkylphenyl ketones. The subsequent reactions occur with little probability from the triplet 1,4-biradical, due to relatively high barrier or high endothermicity for the spin-conservation triplet pathways. As a result, intersystem crossing to the lowest singlet state takes place prior to the subsequent reactions. Four isomers, $^3$BR*i* (*i* = 1−4), were found to be stable for the triplet 1,4-biradical. The calculated energy gap indicates that the $^3$BR3/$^3$BR2 ratio is close to 1:1, and populations of $^3$BR1 and $^3$BR4 are less than 1% at thermal equilibrium. Like the triplet 1,4-biradical, four stable isomers of $^1$X*i* (*i* = 1−4) were determined in the lowest singlet state. Because of the relatively high barrier (~30 kcal·mol$^{-1}$) on the isomerization pathways, the thermal equilibrium is not established among the four singlet isomers, which is different from the situation for the triplet 1,4-biradical. In this case, the subsequent reactions proceed mainly from the $^1$X2 and $^1$X3 isomers that correspond to $^3$BR2 and $^3$BR3. There is only one predominant pathway from the $^1$X2 isomer, namely, the reversed-H shift to the initial reactant of *o*-acetylphenylacetic acid. However, several possible pathways exist for the $^1$X3 deactivation: intramolecular cyclization, unimolecular decarboxylation, and the parent acid-catalyzed bimolecular decarboxylation. The unimolecular decarboxylation is not in competition with the cyclization. But the cyclization reaction is prevented by the parent acid-catalyzed bimolecular decarboxylation, which is responsible for the products of $CO_2$ and *o*-acyltoluene observed experimentally. The $^1$X3/$^1$X2 ratio is nearly equal to that for $^3$BR3/$^3$BR2, which indicates that the decarboxylation reaction has a quantum yield close to 0.5. The *o*-acyltoluene product was isolated, and its yield was experimentally estimated to be in the 50% range.

## Introduction

Photoinduced decarboxylation is of great interest in synthetic chemistry, pharmaceuticals and agriculture[1] and occurs in a variety of carboxylic acids and compounds containing the carboxyl moiety. In particular, the UV light-induced decarboxylation of various α-arylcarboxylic acids has attracted great attention,[2−6] since several α-arylpropionate salts were found to be nonsteroidal anti-inflammatory agents and they have a variety of biochemical and pharmacological applications. Two mechanisms,[1,2] which involve the $\pi,\pi^*$ excited singlet state of the aromatic moiety,


Published on Web 02/03/2010 DOI: 10.1021/jo902593s

have been identified for photoinduced decarboxylation of α-arylcarboxylic acid in the polar solvents, where proton transfer occurs from the acid to the solvent prior to the photoinduced decarboxylation.

**SCHEME 1**

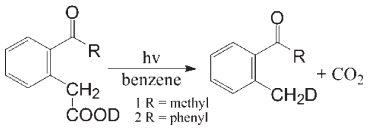


Wagner and co-workers[3] discovered that UV irradiation of *o*-acetylphenylacetic acid (APAA) causes loss of $CO_2$ in nonpolar solvent (benzene), and the isotopic labeling experiments revealed that the O-deuterated acids yield deuterated *o*-acyltoluene products (Scheme 1). Photoinduced decarboxylation was not observed to occur for the *m*- and *p*-acetylphenylacetic acids in benzene. Inspired by the well-known mechanism for photoenolization[7−9] of *o*-alkylphenyl ketones, Wagner and co-workers suggested a radical-like mechanism[3] in which the n,$\pi^*$ excited ketone first abstracts a hydrogen atom from the ortho benzylic carbon to generate excited xylylenol intermediates.[10,11] The excited intermediates relax to the ground state via intersystem crossing (ISC), which is followed by the decarboxylation in the ground state.

**SCHEME 2**

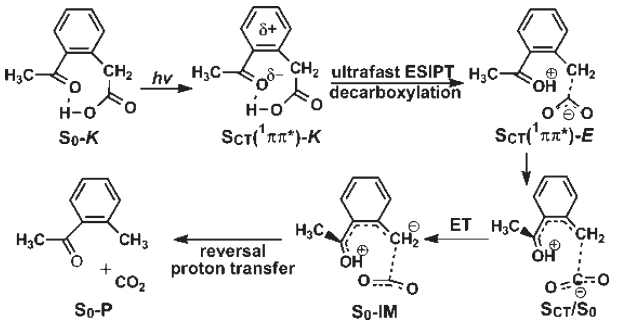


Recently, we reported a new mechanism for the photoinduced decarboxylation of *o*-acetylphenylacetic acid by the combined CASPT2 and CASSCF calculations (Scheme 2).[12] The decarboxylation was found to be an ultrafast process, which is triggered by excited-state intramolecular proton transfer. The reaction starts from the charge-transfer $\pi\pi^*$ singlet state and passes through the conical intersection to the ground state. Subsequent electron transfer and proton transfer in the ground state lead to formation of the final products.

In the present work, we examined theoretically the radical-like mechanism suggested by Wagner and co-workers[3] for the light-induced decarboxylation of *o*-acetylphenylacetic acid. Upon irradiation at ~300 nm, the APAA molecules are excited to the $S_1$ state and then decay rapidly to $T_1$ state via the $S_1/T_2/T_1$ three-surface intersection. An efficient 1,5-H shift occurs from the $T_1$ state, yielding 1,4-biradical in the triplet state. The equilibrium populations of the triplet isomers for the 1,4-biradical control the subsequent formation of isomers in the lowest singlet state, while conformers of the singlet isomers determine the ratio of the reversed-H shift to the initial reactant and the parent acid-catalyzed bimolecular decarboxylation to the products of $CO_2$ and *o*-acyltoluene. We believe that the reported results here provide new insights into the radical-like mechanism of the light-induced APAA decarboxylation.

## Computational Details

The complete active space self-consistent field (CASSCF) method[13] is employed to optimize stationary structures on the $S_0$, $T_1$, $S_1$, $T_2$, and $S_2$ states of APAA because the CASSCF wave function has sufficient flexibility to model the changes in electronic structure upon electronic excitation. Ten electrons in nine orbitals were chosen as the active space for the present CASSCF calculations of APAA in different electronic states, referred to as CAS(10,9) hereafter. The active orbitals are composed of three $\pi$ and $\pi^*$ orbitals in the aromatic ring, the C=O $\pi$ and $\pi^*$ orbitals, and one oxygen nonbonding orbital. For 1,4-biradicals produced by the 1,5-H shift, the CASSCF calculation was performed with 10 electrons in eight orbitals, without the C=O $\pi^*$ orbital in the CAS(10,9) active space. The state-averaged CASSCF method[14] was used to determine geometry on intersection space of two electronic states with the same spin multiplicity, while the minimum-energy crossing points between the singlet and triplet states were optimized by using Slater determinants in the state-averaged CASSCF calculations.[15] The spin−orbit coupling at the singlet−triplet crossing point was calculated with a one-electron approximation for the spin−orbital coupling operator.[16] All of the CASSCF calculations were performed with the 6-31G* basis set.

The B3LYP method[17] has been demonstrated to be computationally efficient and can give a satisfactory reproduction of the observed structures, barrier heights, and transition energies,[18,19] which, together with the 6-31G* and 6-311G** basis sets[20] has been first used to locate the energy-minimum structures of the APAA molecule in the ground state ($S_0$) with and without $C_s$ symmetry constraint. Then, the equilibrium geometries and transition-state (TS) structures in the lowest

(1) Budac, D.; Wan, P. *J. Photochem. Photobiol. A: Chem* **1992**, *67*, 135–166. and references therein.
(2) Epling, G. A.; Lopes, A. *J. Am. Chem. Soc*. **1977**, *99*, 2700–2704.
(3) Sobczak, M.; Wagner, P. J. *Org. Lett*. **2002**, *4*, 379–382.
(4) Bosca, F.; Miranda, M. A.; Carganico, G.; Mauleon, D. *Photochem. Photobiol*. **1994**, *60*, 96–101.
(5) Costanzo, L. L.; Guidi, G. D.; Condorelli, G.; Cambria, A.; Fama, M. *Photochem. Photobiol*. **1989**, *50*, 359–365.
(6) Musa, K. A. K.; Matxain, J. M.; Eriksson, L. A. *J. Med. Chem*. **2007**, *50*, 1735–1743.
(7) Wagner, P. J.; Subrahmanyam, D.; Park, B. S. *J. Am. Chem. Soc*. **1991**, *113*, 709–710.
(8) Wagner, P. J.; Sobczak, M.; Park, B.-S. *J. Am. Chem. Soc*. **1998**, *120*, 2488–2489.
(9) Small, R. D.; Scaiano, J. C. *J. Phys. Chem*. **1977**, *81*, 2126–2131.
(10) Yang, N. C.; Rivas, C. *J. Am. Chem. Soc*. **1961**, *83*, 2213–2213.
(11) Zwicker, E. F.; Grossweiner, L. I.; Yang, N. C. *J. Am. Chem. Soc*. **1963**, *85*, 2671–2672.
(12) Ding, L.; Chen, X.; Fang, W.-H. *Org. Lett*. **2009**, *11*, 1495–1498. and references therein.
(13) Schmidt, M. W.; Gordon, M. S. *Annu. Rev. Phys. Chem*. **1997**, *49*, 233–266.
(14) Frisch, M.; Ragazos, I. N.; Robb, M. A.; Schlegel, H. B. *Chem. Phys. Lett*. **1992**, *189* (6), 524–528.
(15) Yamamoto, N.; Vreven, T.; Robb, M. A.; Frisch, M. J.; Bernhard Schlegel, H. *Chem. Phys. Lett*. **1996**, *250*, 373–378.
(16) Abegg, P. W. *Mol. Phys*. **1974**, *27*, 763–7772. Koseki, S.; Schmidt, M. W.; Gordon, M. S. *J. Phys. Chem*. **1992**, *96*, 10768–10775.
(17) Becke, A. D. *J. Chem. Phys*. **1993**, *98*, 5648–5652. Lee, C.; Yang, W.; Parr, R. G. *Phys. Rev. B*. **1988**, *37*, 785–789.
(18) Wiberg, K. B.; Stratmann, R. E.; Frisch, M. J. *Chem. Phys. Lett*. **1998**, *297*, 60–64.
(19) Chen, W.-C.; Yu, C.-H. *J. Chem. Phys*. **2001**, *115*, 7495–7502. and references therein.
(20) Rassolov, V. A.; Ratner, M. A.; Pople, J. A.; Redfern, P. C.; Curtiss, L. A. *J. Comput. Chem*. **2001**, *22*, 976–984.

triplet state ($T_1$) have been optimized at the B3LYP/6-311G** level. The nature of the critical points (equilibrium geometries and transition states) was confirmed by an analytical frequency computation at the same level. The intrinsic reaction coordinate (IRC) calculations have been carried out at the B3LYP/6-311** level with the saddle point structures as the starting points, in order to confirm the optimized saddle point to be on the correct reaction pathway. All the CAS(10,9) and B3LYP calculations reported in this work were performed with the Gaussian 03 package of programs.[21]

## Results and Discussion

**Electronic and Geometric Structures.** There are 16 possible conformers for the APAA molecule in the ground state under $C_s$ symmetry, but none of them is the minimum energy structure. Upon releasing the symmetry constraint, several local minimum conformers were determined by the B3LYP calculations with the two lowest energy conformers (**A** and **B**) given in Scheme 3. The energy difference between **A** and **B** is about 1.0 kcal·mol$^{-1}$, which is dependent on the methods used. There is a strong H-bond between the $CH_3CO$ and COOH groups in the **A** conformer, which is favorable to the proton transfer from the COOH group to the acetyl group.

**SCHEME 3**

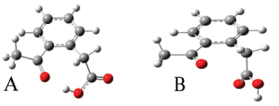


Phototriggered intramolecular proton transfer in the **A** conformer and subsequent decarboxylation have been studied previously.[12] It can be seen that the proton transfer from the COOH group to the acetyl group is blocked in the **B** structure, but the 1,5-H shift between the C7 and O11 atoms is opened in this structure (atom-labeling scheme in Figure 1), the radical-like mechanism proposed in the experimental study.[3] In the present paper, we chose the **B** conformer as the initial structure to investigate photoinduced decarboxylation and related reactions.

The CAS(10,9)/6-31G*-optimized structures for the APAA molecule in the $S_0$, $T_1$, $T_2$, $S_1$, and $S_2$ states are schematically shown in Figure 1 along with the selected bond parameters. The CAS(10,9)/6-31G*-optimized bond parameters for the $S_0$ state are similar to those obtained by the B3LYP/6-311G** optimizations. The conjugation character of the $\pi$ system is well described by the CAS(10,9)/6-31G* and B3LYP/6-311G** calculations. Upon electronic excitation to the $S_1$ state, the most striking change in structure is

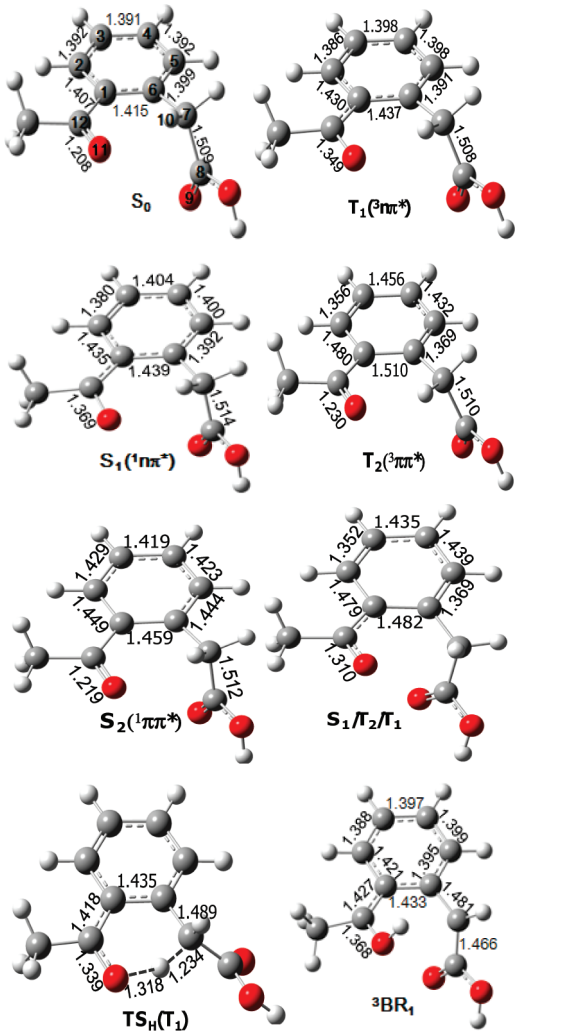


**FIGURE 1.** Schematic stationary and intersection structures along with the key bond lengths (in Å); the atom-labeling scheme illustrated in the $S_0$ structure.

associated with the C12−O11 bond length, which is 1.208 Å in $S_0$ and becomes 1.369 Å in the $S_1$ structure. Meanwhile, the C1−C12 bond length is decreased to 1.398 Å from 1.497 Å in the $S_0$ state. The CAS(10,9)/6-31G*-calculated wave functions clearly show that the $S_1$ state is of $^1n\pi^*$ character, which is mainly localized in the $CH_3CO$ group. As shown in Figure 1, the bond parameters in the $T_1(^3n\pi^*)$ state are very similar to those in the $S_1(^1n\pi^*)$ state.

Unlike the $n\rightarrow\pi^*$ excitation, which is mainly localized in the carbonyl group, the structure of the aromatic ring is remarkably changed by the $\pi\rightarrow\pi^*$ electronic transition. In the $T_2(^3\pi\pi^*)$ state, the C2−C3 and C5−C6 bond distances are 1.356 and 1.369 Å, respectively, which are mainly of double-bond character. The other C−C bonds in the aromatic ring exhibit clear single bond nature. The geometric feature of the $T_2(^3\pi\pi^*)$ state is consistent with its electronic structure plotted in Scheme 4. The $S_2(^1\pi\pi^*)$ state is quite different from the $T_2(^3\pi\pi^*)$ state in structure. Two unpaired electrons are delocalized into the whole aromatic ring, which results in a visible increase of the ring C−C bonds in the $S_2$ state. It should be pointed out that the $\pi\rightarrow\pi^*$ transition has little influence on structure and nature of the $CH_3CO$ group.

(21) Frisch, M. J.; Trucks, G. W.; Schlegel, H. B.; Scuseria, G. E.; Robb, M. A.; Cheeseman, J. R.; Montgomery, J. A. J.; Vreven, T.; Kudin, K. N.; Burant, J. C.; Millam, J. M.; Iyengar, S. S.; Tomasi, J.; Barone, V.; Mennucci, B.; Cossi, M.; Scalmani, G.; Rega, N.; Petersson, G. A.; Nakatsuji, H.; Hada, M.; Ehara, M.; Toyota, K.; Fukuda, R.; Hasegawa, J.; Ishida, M.; Nakajima, T.; Honda, Y.; Kitao, O.; Nakai, H.; Klene, M.; Li, X.; Knox, J. E.; Hratchian, H. P.; Cross, J. B.; Bakken, V.; Adamo, C.; Jaramillo, J.; Gomperts, R.; Stratmann, R. E.; Yazyev, O.; Austin, A. J.; Cammi, R.; Pomelli, C.; Ochterski, J. W.; Ayala, P. Y.; Morokuma, K.; Voth, G. A.; Salvador, P.; Dannenberg, J. J.; Zakrzewski, V. G.; Dapprich, S.; Strain, M. C.; Daniels, A. D.; Farkas, O.; KMalick, D.; Rabuck, A. D.; Raghavachari, K.; Foresman, J. B.; Ortiz, J. V.; Cui, Q.; Baboul, A. G.; Clifford, S.; Cioslowski, J.; Stefanov, B. B.; Liu, G.; Liashenko, A.; Piskorz, P.; Komaromi, I.; Martin, R. L.; Fox, D. J.; Keith, T.; Al-Laham, M. A.; Peng, C. Y.; Nanayakkara, A.; Challacombe, M.; Gill, P. M. W.; Johnson, B.; Chen, W.; Wong, M. W.; Gonzalez, C.; Pople, J. A. *Gaussian03, revision B.03*; Gaussian, Inc.: Wallingford, CT, 2004.

**SCHEME 4**

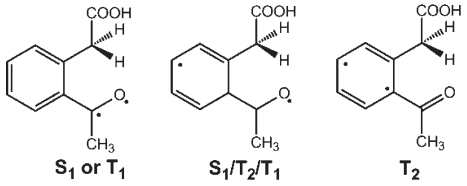


The adiabatic excitation energies to $T_1(^3n\pi^*)$, $T_2(^3\pi\pi^*)$, $S_1(^1n\pi^*)$, and $S_2(^1\pi\pi^*)$ were calculated to 74.3, 76.9, 77.0, and 103.8 kcal·mol$^{-1}$, respectively, at the CAS(10,9)/6-31G* level, which is in good agreement with the corresponding band origin of 73.9, 76.9, 77.9, and 101.2 kcal·mol$^{-1}$ for acetophenone.[22−25] Since the energy difference is very small among the $S_1(^1n\pi^*)$, $T_1(^3n\pi^*)$, and $T_2(^3\pi\pi^*)$ states, it can be expected that the three states may intersect in the Franck−Condon region, which is confirmed by the state-averaged CASSCF calculation. The singlet and triplet surface crossing was optimized by using Slater determinant wave functions in the state-averaged CASSCF calculations and was identified as the $^1n\pi^*$ and $^3\pi\pi^*$ surface crossing ($^1n\pi^*/^3\pi\pi^*$). Similarly, the minimum energy intersection between the two triplet surfaces was determined as one between the $^3\pi\pi^*$ and $^3n\pi^*$ surfaces ($^3\pi\pi^*/^3n\pi^*$). The optimized structures show that $^1n\pi^*/^3\pi\pi^*$ and $^3\pi\pi^*/^3n\pi^*$ are indistinguishable from one another in structure and the two crossing points have the same energy. Actually, the $^1n\pi^*$, $^3\pi\pi^*$, and $^3n\pi^*$ states intersect in the Franck−Condon region ($S_1/T_2/T_1$) for the APAA molecule and the optimized minimum energy $S_1/T_2/T_1$ structure is only 2.5 kcal·mol$^{-1}$ above the $S_1$ minimum. The $S_1/T_2/T_1$ structure is shown in Figure 1, and the detailed structural parameters are available in the Supporting Information. In the $S_1(^1n\pi^*)$ and $T_1(^3n\pi^*)$ structures, two singly occupied electrons are mainly populated in the carbonyl C12 and O11 atoms, while two singly occupied electrons are mainly in the aromatic ring in the $T_2(^3\pi\pi^*)$ structure. As shown in Scheme 4, the $S_1/T_2/T_1$ electronic structure is located between $S_1(T_1)$ and $T_2$ with the two unpaired electrons distributed in the O11 atom and the aromatic ring, respectively. As discussed in the previous studies,[26,27] there is no first-order spin−orbit coupling between $S_1(^1n\pi^*)$ and $T_1(^3n\pi^*)$, and the direct $S_1(^1n\pi^*)\rightarrow T_1(^3n\pi^*)$ intersystem crossing (ISC) takes place with low efficiency. However, the $T_2(^3\pi\pi^*)$ state acts as a relay and enables the $S_1(^1n\pi^*)\rightarrow T_1(^3n\pi^*)$ ISC to occur with high efficiency in the vicinity of the $S_1/T_2/T_1$ intersection. Using the state-averaged CASSCF calculated wave function, the spin−orbit coupling matrix element at the $S_1/T_2/T_1$ intersection point was calculated to be 52.9 cm$^{-1}$ with a one-electron approximation for the spin−orbital coupling operator, which provides a quantitative assessment of the effectiveness of the $S_1\rightarrow T_1$ ISC process at the $S_1/T_2/T_1$ intersection.

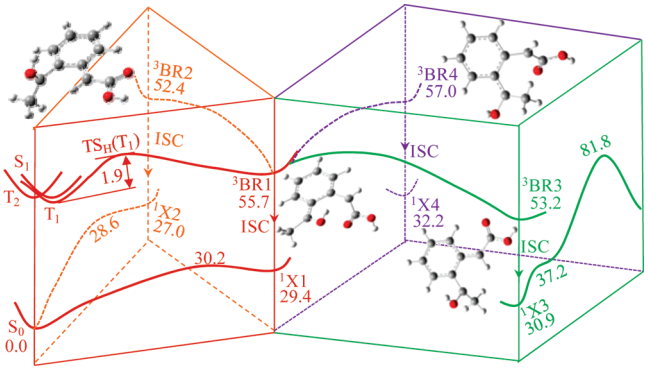


**FIGURE 2.** 1,5-H shift and the subsequent processes.

Actually, the three-surface intersection is a common feature for many aromatic carbonyl compounds with a nearly constant structure[26,27] and holds the key to understanding much of the relaxation dynamics of the $S_1$ state.

**1,5-H Shift Reaction.** 1,5-H shift reaction (Norrish type II reaction)[28] has been confirmed to occur on the $T_1$ state for most aromatic ketones or aldehydes in previous studies.[26,27,29−34] The existence of the $S_1/T_2/T_1$ intersection for APAA indicates that the $S_1$ state relaxes to the $T_1$ state efficiently. A transition state was found by the UB3LYP/6-311G** calculation and confirmed to be the first-order saddle point for 1,5-H shift on the $T_1$ pathway. The transition state, referred to as $TS_H(T_1)$ in Figure 1, has a six-membered structure that is nearly coplanar with the phenyl ring. In the $TS_H(T_1)$ structure, the C7−H10 distance is increased to 1.230 Å and the H10−O11 bond is partially formed with the H10−O11 distance of 1.30 Å. The barrier height for the 1,5-H shift was calculated to be 1.9 kcal·mol$^{-1}$ on the $T_1$ pathway at the UB3LYP/6-311G** level, which indicates that the 1,5-H shift occurs very easily along the triplet pathway. The 1,5-H shift was inferred to have a rate constant larger than $10^9$ s$^{-1}$ for the triplet *o*-alkylphenyl ketones.[35]

The 1,5-H shift reaction primarily gives rise to a 1,4-biradical in the lowest triplet state. Four isomers for the 1,4-biradical in the triplet state, referred to as $^3BRi$ ($i=1-4$) in Figure 2, were determined by the UB3LYP/6-311G** and CAS(10,9)/6-31G* calculations, which originate from rotation of the CHCOOH group around C6−C7 bond and the C(OH)CH$_3$ group around the C1−C12 bond. The $^3$BR2 isomer is the most stable with the relative energies of 0.8, 3.3, and 4.7 kcal·mol$^{-1}$ at the UB3LYP/6-311G** level for $^3$BR3, $^3$BR1, and $^3$BR4, respectively. The UB3LYP/6-311G** calculations indicate that the $^3$BR3 decarboxylation has a barrier of 38.8 kcal·mol$^{-1}$ and the Norrish−Yang cyclization[28] is endothermic by 69.1 kcal·mol$^{-1}$ on the triplet pathway. Thus, the spin-conservation reactions occur

(22) Ridley, J. E.; Zerner, M. C. *J. Mol. Spectrosc.* **1979**, *76*, 71–85.
(23) Ohmori, N.; Suzuki, T.; Ito, M. *J. Phys. Chem.* **1988**, *92*, 1086–1093.
(24) Silva, C. R.; Reilly, J. P. *J. Phys. Chem.* **1996**, *100* (43), 17111–17123. and references therein.
(25) Warren, J. A.; Bernstein, E. R. *J. Chem. Phys.* **1986**, *85*, 2365–2367.
(26) Fang, W.-H.; Phillips, D. L. *Chem. Phys. Chem.* **2002**, *3*, 889–892. Fang, W.-H.; Phillips, D. L. *J. Theor. Comput. Chem.* **2003**, *2*, 23–31. Wang, Y.-W.; He, H.-Y.; Fang, W.-H. *THEOCHEM* **2003**, *634*, 281–287. He, H.-Y.; Fang, W.-H.; Phillips, D. L. *J. Phys. Chem. A* **2004**, *108*, 5386–5392.
(27) Fang, W.-H. *Acc. Chem. Res.* **2008**, *41*, 452–457. Ding, L.; Shen, L.; Chen, X.; Fang, W.-H. *J. Org. Chem.* **2009**, *74*, 8956–8962.
(28) Yang, N. C.; Yang, D. H. *J. Am. Chem. Soc.* **1958**, *80*, 2913–2914.
(29) Wagner, P. J. *Acc. Chem. Res.* **1971**, *4*, 168–177.
(30) Wagner, P. J.; McGrath, J. M. *J. Am. Chem. Soc.* **1972**, *94*, 3849–3851.
(31) Lewis, F. D.; Hilliard, T. A. *J. Am. Chem. Soc.* **1972**, *94*, 3852–3858.
(32) Wagner, P. J. *Acc. Chem. Res.* **1989**, *22*, 83–91.
(33) Zepp, R. G.; Gumz, M. M.; Miller, W. L.; Gao, H. *J. Phys. Chem. A* **1998**, *102*, 5716–5723.
(34) Takahashi, K.; Watanabe, T.; Kohtani, S.; Nakagaki, K. *J. Photochem. Photobiol. A: Chem* **2007**, *186*, 290–297.
(35) Wagner, P. J.; Chen, C.-P. *J. Am. Chem. Soc.* **1976**, *98*, 239–241.

**SCHEME 5**

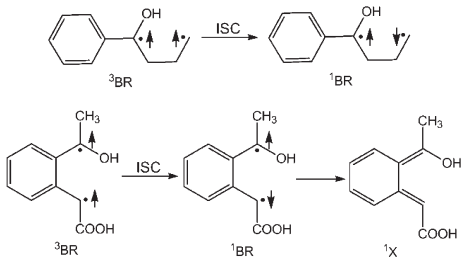


with little probability for the triplet 1,4-biradical. As will be discussed below, intersystem crossing (ISC) from the triplet 1,4-biradical to the lowest singlet state takes place on a time scale of nanosecond. In this case, thermal equilibrium of the four isomers can be established for the triplet 1,4-biradical. The calculated energy gap (2.5 − 3.6 kcal·mol$^{-1}$) indicates that populations of $^3$BR1 and $^3$BR4 are less than 1% at thermal equilibrium.

Four intersection structures, $^3$BR$i$/$^1$X$i$ ($i$ = 1−4), were determined by the state-averaged CAS(10,8)/6-31G* calculations, which connects the corresponding triplet 1,4-biradical ($^3$BR$i$, $i$ = 1−4) and the singlet state ($^1$X$i$, $i$ = 1−4). The $^3$BR$i$/$^1$X$i$ intersection is similar to the $^3$BR$i$ 1,4-biradical in structure and has its energy in the range of 1.0−5.7 kcal·mol$^{-1}$ with respect to the minimum of the triplet 1,4-biradical. If the intersystem crossing via the $^3$BR$i$/$^1$X$i$ ($i$ = 1−4) intersection was a spin-allowed process, it would take place on a time scale of picosecond. However, the spin−orbit coupling matrix elements at the $^3$BR$i$/$^1$X$i$($i$ = 1−4) intersection structures were calculated to be about 0.2 cm$^{-1}$ by using one-electron spin−orbit Hamiltonian with effective nuclear charges[16] and the state-averaged CAS-(10,8)/6-31G* wave functions. A probability factor (transition probability per passage through the crossing seam) from the triplet to singlet state is estimated to be ∼10$^{-5}$ by the Landau−Zener law.[36] As a result, the intersystem crossing via the $^3$BR$i$/$^1$X$i$ ($i$ = 1−4) intersection has a rate constant of ∼10$^7$ s$^{-1}$, which is consistent with a lifetime of ∼10$^{-7}$ s observed for the triplet 1,4-biradical in the solution phase.[37]

**The Subsequent Cyclization, Reversed-H Shift, and Decarboxylation.** The 1,4-biradical in the lowest singlet state is unstable for APAA and rearranges to a closed-shell structure very easily, as shown in Scheme 5. This is different from those observed for butyrophenone and valerophenone[26,27] where the singlet 1,4-biradical is stable with high reactivity. Four singlet structures of $^1$X$i$($i$ = 1−4) were confirmed to be minima in the ground state by the B3LYP/6-311G** calculations. As shown in Figure 2, the $^1$X2 isomer is the most stable with the relative energy of 2.4, 3.9, and 5.2 kcal·mol$^{-1}$ for $^1$X1, $^1$X3, and $^1$X4, respectively. But isomerization among them results in a breakage of the C=C $\pi$ bond and does not proceed easily. The B3LYP/6-311G** calculations reveal that the reversed-H shift to the initial reactant of *o*-acetylphenyl-acetic acid has the barrier height of 0.8 and 1.6 kcal·mol$^{-1}$ from $^1$X1 and $^1$X2, respectively. It is evident that other processes starting from the $^1$X1 and $^1$X2 isomers are not in competition with the reversed-H shift. The $^1$X3 and $^1$X4 isomers have a favor structure for the cyclization. Two transition states were found for the cyclization reactions with $^1$X3 and $^1$X4 as reactants, and the barriers were respectively calculated to be 19.0 and 17.7 kcal·mol$^{-1}$ at the B3LYP/-6-311G** level. This shows that the cyclization reactions can take place with considerable efficiency upon photoexcitation at 300 nm (∼95.3 kcal·mol$^{-1}$).

As pointed out before, the $^1$X1 and $^1$X2 isomers return to the initial reactant rapidly. Thus, the decarboxylation reaction may start from the $^1$X3 and $^1$X4 isomers, which involves a rotation of the COOH group and a concerted 1,3-H shift and the C−C bond cleavage. It can be expected that the decarboxylation reaction proceeds with considerable difficulty. The evidence for this comes from the B3LYP/-6-311G** calculated barrier height of 50.9 kcal·mol$^{-1}$ from $^1$X3 and 48.8 kcal·mol$^{-1}$ from $^1$X4. Although the decarboxylation reactions from $^1$X3 and $^1$X4 are accessible in energy upon photoexcitation at 300 nm, they are not in competition with the cyclization reactions. It should be pointed out that the $CO_2$ product has been observed upon near-UV (∼300 nm) irradiation of *o*-acetylphenylacetic acid in benzene.[3]

Here, we explore the possibility of the APAA-assisted decarboxylation of $^1$X3. The APAA-$^1$X3 complex was optimized at the B3LYP/6-311G** level, and the optimized structure is shown in Figure 3, along with intermolecular H-bond distances. It was found that a concerted double-proton transfer occurs very easily in the APAA−$^1$X3 complex. A transition state was characterized for the double-proton transfer, referred to as TS-2H in Figure 3. The IRC and frequency calculations validated TS-2H to be the first-order saddle point on the pathway from the APAA-$^1$X3 complex to an intermediate (INT1). The double-proton transfer has to overcome a barrier of 9.8 kcal·mol$^{-1}$ at the B3LYP/6-311G** level. The INT1 structure was optimized and confirmed to be a minimum by frequency calculation. The calculated Mulliken atomic charge distribution reveals that INT1 is partially of zwitterionic character with about −0.5 atomic charge in the O9−C8−O13 moiety. The corresponding +0.5 atomic charge is mainly localized the aromatic ring. The other feature of the INT1 structure is associated with the C7−C8 distance of 1.615 Å (Figure 3), which is much longer than general C−C single bond. This gives us a hint that the decarboxylation from INT1 proceeds easily. A transition state was determined for the decarboxylation from INT1, labeled TS-$CO_2$ hereafter. TS-$CO_2$ was confirmed to be the first-order saddle point and is less than 1.0 kcal·mol$^{-1}$ above the INT1 minimum. Actually, TS-$CO_2$ is lower than INT1 in energy after inclusion of zero-point energy correction. The optimized structures and calculated energies provide strong evidence that the decarboxylation from INT1 proceeds very easily. After loss of $CO_2$, intramolecular hydrogen transfer occurs, leading to the final products of *o*-acyltoluene and *o*-acetylphenylacetic acid. It is obvious that the cyclization reactions of $^1$X3 and $^1$X4 are prevented by the parent acid-catalyzed decarboxylation, which is responsible for the $CO_2$ product observed experimentally.[3]

**Mechanistic Aspects.** The photoinduced decarboxylation processes of *o*-acetylphenylacetic acid in near-UV region are

(36) Harvey, J. N.; Aschi, M. *Phys. Chem. Chem. Phys.* **1999**, *1*, 5555–5563. and references therein.
(37) Das, P. K.; Encinas, M. V.; Small, R. D.; Scaiano, J. C. *J. Am. Chem. Soc.* **1979**, *101*, 6965–6970.

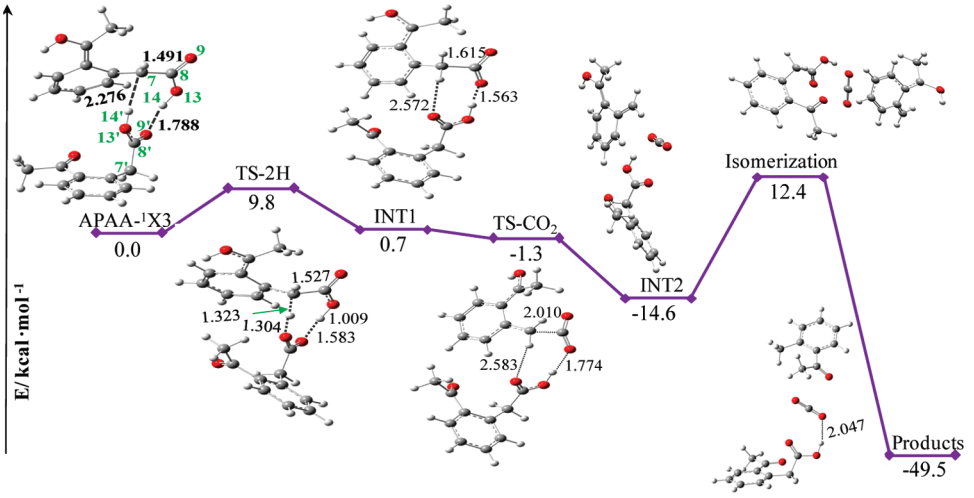


**FIGURE 3.** Parent acid-catalyzed bimolecular decarboxylation processes.

**SCHEME 6**

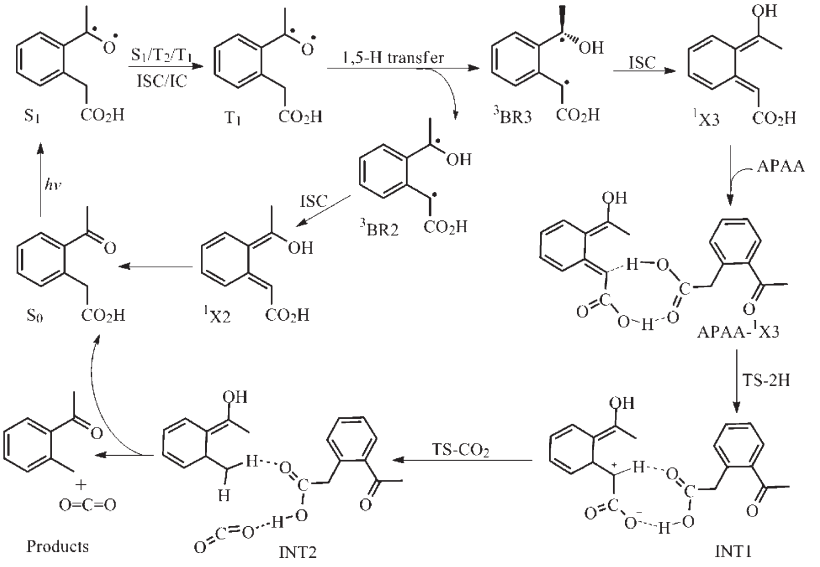


summarized in Scheme 6. Near-UV (~300 nm) irradiation of *o*-acetylphenylacetic acid (APAA) drives the molecule to the $S_1(^1n\pi^*)$ state. From this state, the APAA molecule can decay to the $T_1(^3n\pi^*)$ state via the $S_1/T_2/T_1$ three-surface intersection. As pointed out before, the three-surface intersection is only 2.5 kcal·mol$^{-1}$ above the $S_1$ minimum. In addition, there exists a small difference in the $S_1$ and $S_1/T_2/T_1$ structures (Scheme 4), which mainly results from the redistribution of the conjugation $\pi$ electrons. In view of the structures and the energies found here for the $S_1$ Franck−Condon (FC) point, the $S_1$ minimum, and the $S_1/T_2/T_1$ intersection, the $FC(S_1) \rightarrow S_1/T_2/T_1$ relaxation is a very rapid process. Direct $S_1(^1n\pi^*) \rightarrow T_1(^3n\pi^*)$ intersystem crossing would be expected to occur with a low efficiency because there is no first-order spin−orbit coupling for the $S_1 \rightarrow T_1$ transition.[26] However, the $S_1(^1n\pi^*) \rightarrow T_2(^3n\pi^*)$ ISC process happens with high efficiency due to a strong spin−orbit interaction.[26] Thus, the $T_2(^3\pi\pi^*)$ state acts as a relay and enables the $S_1(^1n\pi^*) \rightarrow T_1(^3n\pi^*)$ ISC to occur with high efficiency in the vicinity of the $S_1/T_2/T_1$ intersection.

Once in the $T_1$ state, the 1,5-H shift becomes a dominant channel, due to a barrier of 1.9 kcal·mol$^{-1}$ on the pathway to the triplet 1,4-biradical, which is in good agreement with the rate constant of about $10^{10}$ s$^{-1}$ inferred experimentally for *o*-alkylphenyl ketones.[35] Because of relatively high barriers or high endothermicity, the spin-conservation reactions starting from the triplet 1,4-biradical take place with little probability. The ISC process from the triplet 1,4-biradical to the lowest singlet state was estimated to occur on a time scale of nanosecond. As a result of these, thermal equilibrium is established among the four isomers of the triplet 1,4-biradical. The $^3$BR1 and $^3$BR4 isomers are 2.5−4.6 kcal·mol$^{-1}$ higher than the $^3$BR2 and $^3$BR3 isomers in energy. The calculated energy gap indicates that populations of $^3$BR1 and $^3$BR4 are less than 1% at thermal equilibrium. In this case, the ISC process takes place mainly from equilibrium populations of the $^3$BR2 and $^3$BR3 isomers, which yields two singlet isomers of $^1$X2 and $^1$X3 with the $^1$X3/$^1$X2 ratio close to 0.5.

There is only one predominant pathway from the $^1$X2 isomer, namely, the reversed-H shift to the initial reactant of

*o*-acetylphenylacetic acid, but several possible pathways exist for the $^1$X3 deactivation/isomerization to $^1$X2, intramolecular cyclization, unimolecular decarboxylation, and the APAA-assisted bimolecular decarboxylation. The unimolecular decarboxylation has a barrier of 50.9 kcal·mol$^{-1}$ relative to the $^1$X3 zero-level, which is much higher than those (~20 kcal·mol$^{-1}$) for the cyclization and the isomerization to $^1$X2. However, the APAA-assisted bimolecular decarboxylation has to overcome a barrier of about 10.0 kcal·mol$^{-1}$ to the $CO_2$ product. It is evident that the APAA-assisted decarboxylation is the dominant channel from $^1$X3, which is responsible for formation of the products of $CO_2$ and *o*-acyltoluene observed experimentally.[3] The $^1$X3/$^1$X2 ratio of about 0.5 indicates that the decarboxylation reaction has a quantum yield of about 0.5, which is consistent with the experimental findings.[3]

**Acknowledgment.** This work was supported by grants from the NSFC (Grant No. 20720102038) and from the Major State Basic Research Development Programs (Grant No. 2004CB719903).

**Supporting Information Available:** Cartesian coordinates and absolute energies of the stationary and intersection structures. This material is available free of charge via the Internet at http://pubs.acs.org.